Contract No.:

This manuscript has been authored by Savannah River Nuclear Solutions (SRNS), LLC under Contract No. DE-AC09-08SR22470 with the U.S. Department of Energy (DOE) Office of Environmental Management (EM).

Investigations of Uranyl Fluoride Sesquihydrate ($UO_2F_2 \cdot 1.57H_2O$): Combining ^{19}F Solid-State MAS NMR Spectroscopy and GIPAW Chemical Shift Calculations

Michael A. DeVore II[A], *Christopher A. Klug*[B], *Maria R. Kriz*[A], *Lindsay E. Roy*[A], *and Matthew S. Wellons*[*,A]

Contributions from [A] Savannah River National Laboratory, P. O. Box A, Aiken, SC 29808 and

[B] U.S. Naval Research Laboratory, 4555 Overlook Ave. SW Washington, DC, 20375

RECEIVED DATE (to be automatically inserted after your manuscript is accepted if required according to the journal that you are submitting your paper to)

[*] To whom correspondence should be addressed (matthew.wellons@srnl.doe.gov)

Abstract

High-resolution ^{19}F magic angle spinning (MAS) NMR spectra were obtained for the uranium-bearing solid, uranyl fluoride ($UO_2F_2 \cdot 1.57H_2O$). While there are seven distinct crystallographic fluorine sites, the ^{19}F NMR spectrum reveals six peaks at -33.3, 9.1, 25.7, 33.0, 39.0, and 48.2 ppm, with the peak at 33.0 ppm twice the intensity of all the others and therefore corresponding to two sites. To assign the peaks in the experimental spectra to crystallographic sites, ^{19}F chemical shifts were calculated by using the GIPAW (Gauge Including Projector Augmented Waves) plane-wave pseudopotential approach for a DFT-optimized crystal structure. The peak assignments from DFT are consistent with 2D double-quantum (DQ) ^{19}F MAS NMR experiments.

1. Introduction

Magic-angle spinning nuclear magnetic resonance (MAS NMR) spectroscopy has become a powerful tool for the interrogation of the local chemical environment of crystalline solids, resulting in enhanced structural characterization that complements diffraction-based methods.[1] When coupled with density functional theory (DFT) methods, assignment of spectral resonances of complex inorganic solids can be realized and improved crystal structures are often obtained.[1] While this methodology is successful for interpretation and prediction of the spectral assignments for several main group and transition metal solids, applicability to compounds containing heavy elements such as the actinides wherein spectral features are caused by relativistic effects on the chemical shift tensor is still difficult.[2] Schreckenbach and coworkers have extended the theoretical calculation of NMR chemical shifts to the actinides for simple molecules, but the methodology has not been rigorously tested using DFT methods incorporating periodic boundary conditions.[3-4] However, there have been recent applications of the GIPAW (Gauge Including Projector Augmented Waves) plane-wave pseudopotential approach to a variety of solids containing heavy elements, e.g. the fluorides TlF[5] and LaF_3[6], and uranium containing compounds.[7-10]

Detailed structural characterization of actinide solids is of particular importance in the nuclear fuel cycle and nuclear safeguards. Uranyl fluoride, for example, is an important intermediate in the conversion of UF_6 to uranium oxides or metal and has been extensively characterized using bulk characterization techniques such as X-ray powder diffraction and Raman spectroscopic methods.[11-12] The crystal structure is highly dependent on the levels of hydration and various related phases include: α $UO_2F_2 \cdot 1.5H_2O$, β $UO_2F_2 \cdot 1.5H_2O$, and $UO_2F_2 \cdot 2H_2O$.[13-14] Thus far, only the anhydrous (UO_2F_2) and uranyl fluoride sesquihydrate ($UO_2F_2 \cdot 1.57H_2O$) crystal structures have been

characterized by neutron diffraction with the fluorine, oxygen, and uranium atom positions determined.[15-16] Based on the known structural information and the high abundance of ^{19}F, uranyl fluoride sesquihydrate is well-suited for a benchmarking study for a combined MAS NMR and GIPAW analysis.

In this work, we combine high-resolution ^{19}F MAS NMR with the calculation of ^{19}F NMR parameters from first principles for the study of uranyl fluoride sesquihydrate ($UO_2F_2 \cdot 1.57H_2O$) to benchmark the methodology for uranium-bearing solids. In order to achieve high resolution ^{19}F NMR spectra, high spinning frequencies (>25 kHz) are required to minimize the broadening effects due to the high density of fluorine and resulting strong inter-nuclear couplings of the fluorine nuclei. Fortunately, the high sensitivity of ^{19}F NMR compensates for the use of the small volume rotors necessary to achieve high spinning frequencies. The ^{19}F NMR spectral interpretation was aided by the use of the two-dimensional homonuclear correlation technique 2D double-quantum (DQ) MAS NMR which probes the spatial proximities of NMR active nuclei via through-space homonuclear dipolar couplings.[17]

2. Experimental and Computational Details

Materials and Characterization. Uranyl fluoride sesquihydrate ($UO_2F_2 \cdot 1.57H_2O$) was purchased from International Bio-Analytical Industries, Inc. and stored within a desiccating environment to prevent further hydrolysis. A second sample was prepared by Andrew Harter at ORNL that was spectrally indistinguishable from commercial material and used to refine the analysis.

All ^{19}F NMR spectra were obtained using a Varian NMR500 spectrometer operating at a magnetic field strength of 11.7 T where the ^{19}F resonance frequency was roughly 470.6 MHz. A 1.2 mm

double resonance UltraFast MAS NMR probe with a ^{19}F RF magnetic field of 250 kHz corresponding to a $\pi/2$ pulse length of 1 μs was used for all experiments. Samples were loaded into the rotor under a dry nitrogen environment in a glove bag. For 1D ^{19}F NMR spectra, rotor-synchronized Hahn spin echoes were used with a typical delay between scans of at least 8 s. It was generally found that suppression of the background ^{19}F NMR signal was accomplished by increasing the inter-pulse delay, *e.g.*, for a spinning frequency of 50 kHz where the rotor period, T_r, was 20 μs, spectra acquired with an inter-pulse delay of $6T_r$=120 μs showed almost no background signal. In the analysis of the peak intensities, corrections due to spin-spin relaxation, T_2, were used. The 2D double-quantum (DQ) MAS measurements were performed using a spinning frequency of 40 kHz and made use of the back-to-back (BABA) pulse sequence for excitation and reconversion, with a typical excitation/reconversion length of 100 μs (4 rotor periods).[18] All ^{19}F NMR spectra were referenced to powdered Teflon (poly(tetrafluoroethylene) (PTFE)) at -122 ppm with respect to $CFCl_3$ (trichlorofluoromethane) at 0 ppm.

Calculations. Calculations were performed using the CASTEP code in the Materials Studio© suite of programs.[2] The exchange-correlation energy was calculated using Perdew-Burke-Ernzerhof (PBE) modification to the generalized gradient approximation.[19] Previously reported crystallographic data were used for calculations of ^{19}F parameters with optimization of the hydrogen atom positions in the structure.[16] The optimization employed Vanderbilt "ultrasoft" pseudopotentials, a planewave cut-off energy of 650 eV, and integrals over the Brillouin zone were performed using a k-point spacing of 0.08 $Å^{-1}$.[20] The tolerances of energy and gradient convergence were used as their default values. Hydrogen optimizations were performed on the C2/C space group of uranyl fluoride sesquihydrate. NMR calculations were performed using the gauge including projector augmented wave approach (GIPAW) with a cut-off of 700 eV within

CASTEP and "on-the-fly" pseudopotentials obtained by Materials Studio©, and a k-point spacing of 0.04 $Å^{-1}$. Calculations generate the absolute shielding tensor ($\boldsymbol{\sigma}$) and diagonalization of the symmetric part of $\boldsymbol{\sigma}$ yields the three principal components or eigenvalues, σ_{xx}, σ_{yy}, and σ_{zz}. The isotropic shielding, σ_{iso}^{calc}, is given by:

$$\sigma_{iso}^{calc} = \frac{1}{3} Tr\{\boldsymbol{\sigma}\} \quad (1)$$

and the isotropic chemical shift, δ_{iso}^{calc} can be obtained from the isotropic chemical shielding, σ_{iso}^{calc}

$$\delta_{iso}^{calc} = -\left(\sigma_{iso}^{calc} - \sigma_{ref}\right) \quad (2)$$

where σ_{ref} is a reference isotropic shielding. In experiment, this value is obtained by measuring the chemical shift of an external reference sample. For calculations, one option is to perform a calculation for the standard reference compound, *e.g.*, $CFCl_3$. Another is to use an average value determined by comparing calculated ^{19}F isotropic shieldings and experimental ^{19}F isotropic chemical shifts for simple fluorine-containing compounds. There is limited precedent in the literature for comparing NMR parameters with first-principles calculations for uranium solid state compounds.[3-4, 21] Therefore, the approach in this work, as suggested in the literature for ^{19}F NMR of other systems, used a linear scaling of the calculated values to compare to the experimental ^{19}F chemical shifts.[5-6, 22-32]

From the principal components of the symmetric part of the shielding tensor, the shielding anisotropy ($\Delta\sigma_{aniso}^{calc}$), which describes the largest separation from the center of gravity, and asymmetry parameter (η), which describes line shape deviation, can be calculated:

$$\Delta\sigma_{aniso}^{calc} = \sigma_{zz} - \frac{1}{2}(\sigma_{xx} + \sigma_{yy}) \quad (3)$$

$$\eta = \frac{(\sigma_{yy} - \sigma_{xx})}{(\sigma_{zz} - \sigma_{iso})} \quad (4)$$

The shielding anisotropy is then related to the reduced shielding anisotropy, ζ, by equation 5:

$$\zeta = \sigma_{zz} - \sigma_{iso} = \frac{2}{3}\Delta\sigma_{aniso}^{calc} \quad (5)$$

The reduced chemical shift anisotropy and asymmetry parameters are typically the values reported in experiment. Discussion into the use of a scaling factor for the reduced anisotropy will be provided in the text below. The sign of the anisotropy indicates on which side of the isotropic value one can find the largest separation. For these calculations, the ζ value is reported as the absolute value. The principal components of the symmetric shielding tensor are ordered as $|\sigma_{zz} - \sigma_{iso}| \geq |\sigma_{xx} - \sigma_{iso}| \geq |\sigma_{yy} - \sigma_{iso}|$. The raw NMR data generated by CASTEP can be found in in the supplemental information.

3. Results and Discussion

The structure of uranyl fluoride sesquihydrate can be described as a three-dimensional network of corner- and edge-sharing uranyl pentagonal bipyramids. Fluorine atoms are shared within the network and water molecules help to complete the coordination sphere around the uranyl group. Due to the sharing of each fluorine atom, each pentagonal uranyl building group can be considered one $UO_2F_2(H_2O)$ formula unit. There are seven fluorine atoms in the asymmetric unit, defined in

Figure 1. Outer sphere water molecules reside in large channels and allow for extensive hydrogen bonding in the crystal structure.[33]

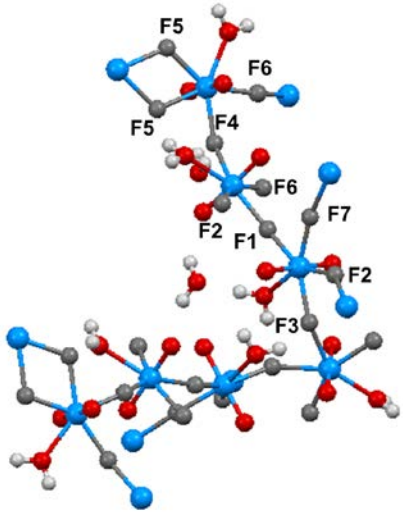

Figure 1: Asymmetric unit ball and stick diagram for $UO_2F_2 \cdot 1.57H_2O$ with unique fluorines labeled. Uranium (blue), Oxygen (red), Fluorine (Gray), Hydrogen (white).

The crystallinity and structure of the uranyl fluoride used in the various NMR characterizations were verified with powder XRD (SI Figure S1). The peak pattern clearly matches the known pattern for $(UO_2F_2{*}H_2O)(H_2O)_{0.571}$ published by Mikhailov *et al.* with no observable unaccounted peaks.[16] After the hydrogen positions were optimized in the calculations, two Rietveld refinements were conducted with and without the geometry optimized hydrogens present in the crystal structure to measure the fit of the pattern. Indeed, the measure of fit (χ) improved for the structure with hydrogen present compared to the structure without from 6.2 to 5.5 (SI Figure S2 and Figure S3). Although hydrogen weakly scatters X-rays, particularly relative to the other atoms present the decrease in χ demonstrates an increased structural consistency between the optimized structure and diffraction measurement.

Figure 2 shows a ^{19}F MAS NMR spectrum obtained using the spinning frequency of 50 kHz. The six center bands were identified by comparing spectra obtained at 40, 50, and 60 kHz and are shown in **Figure 2**(b). The small peaks observed near 0, 25, and -45 ppm are assumed to be due to impurities. Chemical shift tensors for each of the six distinct peaks were extracted using the following procedure: i) each peak in **Figure 2**(a) was fit with a simple Gaussian function; ii) each of the six sets of peaks was fit by comparison with results from the NMR simulation software SIMPSON[34]; iii) an estimate of the T_2 correction was obtained by comparing peak intensities as a function of the inter-pulse delay in the Hahn echo; Examples of these fits are shown in the Supplemental Information and the results are given in **Table 1**. Given that the crystal structure of uranyl fluoride sesquihydrate used as the starting point for the DFT calculations has seven fluorine sites with distinct coordination environments, one of the experimental peaks must correspond to two sites, *i.e.*, it must represent the overlap of two peaks with nearly identical shifts. Taking the peak at 33 ppm as corresponding to two sites, the relative intensities of the remaining five peaks should be 14%, while the peak at 33.0 ppm should have a relative intensity of 29%. The experimental values in **Table 2** are in reasonable agreement with these expectations, although peak 4 is larger than expected while peak 6 is smaller than expected. We will return to this issue once structural assignments have been made.

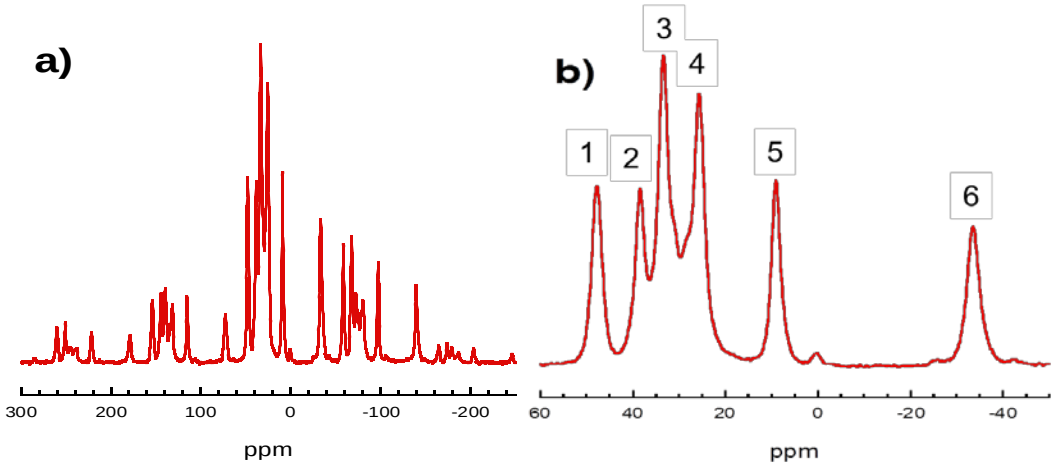

Figure 2: ^{19}F MAS NMR spectra recorded with spinning frequency of 50 kHz a) full spectral width revealing sidebands b) expansion of central region showing only center bands.

Table 1: δ_{iso} , $\delta_{aniso,}$ η, and Relative Intensities deduced from ^{19}F NMR spectra and corresponding simulations—see Supporting Information.

Peak	δ_{iso} (ppm)	δ_{aniso} (ppm)	η	Relative Intensity (%)
1	48.2±1.0	260±20	0.3±0.2	15±1
2	39.0±1.0	260±20	0.3±0.2	14±1
3	33.0±1.0	170±20	0.8±0.2	29±1
4	25.7±1.0	170±20	0.8±0.2	17±1
5	9.1±1.0	230±20	0.5±0.2	13±1
6	-33.3±1.0	230±20	0.5±0.2	12±1

Table 2 Comparisons of experimental ^{19}F chemical shifts (in ppm) with those obtained by theoretical calculations.

δ_{iso}^{expt}	σ_{iso}^{calc}	$\delta_{iso}^{calc,a}$	Atom Label
48.2±1.0	-79.2	45.1	F7
39.0±1.0	-72.7	41.9	F3
33.0±1.0	-63.7, -63.1	37.4, 37.1	F2+F6
25.7±1.0	-31.8	21.5	F1
9.1±1.0	14.0	-1.3	F4
-33.0±1.0	61.5	-25.0	F5

[a] Calculated chemical shifts are scaled using the equation $\delta isocalc = -k(\sigma_{isocalc} - \sigma_{ref})$ where σ_{ref} is 11.34 ppm and the scaling factor, *k*, is 0.4988.

To assign the experimental peaks to crystallographic sites, the measured chemical shifts, $\delta_{iso,\ expt}$ were ordered and plotted against the calculated shieldings, σ_{iso}^{calc}—see **Figure 3**. Using the linear correlation given in Equation 1, calculated chemical shifts are obtained—see **Table 3**.

$$\delta_{iso}^{calc} = -0.4988\left(\sigma_{iso}^{calc} - 11.34\right); \quad R^2 = 0.94 \qquad (6)$$

The slope of the correlation between experimental δ_{iso}^{expt} and calculated σ_{iso}^{calc} deviates significantly from a hypothetical m = -1, as shown in **Figure 3**. For comparison, Zheng et al. obtained a slope of -0.86 for metal fluorides,[22] Griffin et al. obtained a slope of -0.68 in fluorinated hydroxy-silicate[23] and Sadoc et al. obtained a slope of =0.80 for alkali, alkaline earth and rare earth fluorides.[6] The much smaller slope in our case is likely due to a "band gap" problem where there is an incorrect coupling between the HOMO and LUMO uranium electronic states.[35] The uranyl

fluoride uranium atom is nominally in a +6 oxidation state but with covalent bonding character in both the oxygen-uranium axial moiety and fluorine-uranium equatorial plane some fraction of the $[Rn]5f^3 6d^1 7s^2$ electron configuration is occupied. The F5 atom is unique in the structure in that it is incorporated in F-bridged U atoms in the structure with a relatively small U-F-U angle of roughly 114° whereas all other fluorine atoms are singly-bridged and their UFU angles range from 143 to 165°.

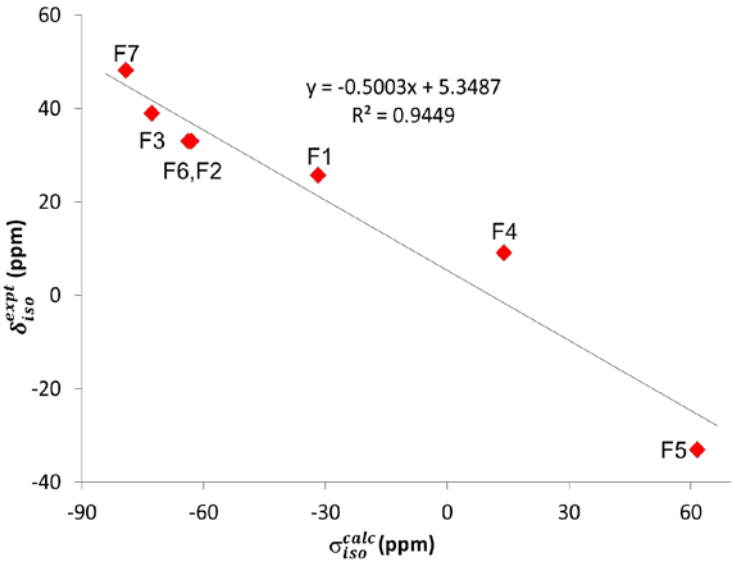

Figure 3: Comparison of experimental ^{19}F isotropic chemical shifts, δ_{iso}^{expt}, and calculated ^{19}F isotropic shieldings, σ_{iso}^{calc}, in ppm.

The other calculated NMR parameters, δ_{aniso}^{calc} and η_{cal}, are compared to experiment in Table 4. When including the scaling factor previously determined from the calculated chemical shifts, the agreement is good. The use of a scaling factor for ζ has been previously proposed and successfully implemented in past work.[2] The accuracy of the asymmetry parameter is not consistent for the

atoms. More work needs to be done to determine the calculation accuracy of the asymmetry parameter for use in actinide solids.

Table 3. Comparisons of experimental ^{19}F chemical shift anisotropy (in ppm) and asymmetry with those obtained by theoretical calculations.

Line	δ_{aniso}^{expt}	$\eta_{exp}{}^{t}$	$\lvert\zeta^{calc}\rvert$	$\lvert\zeta^{calc,scaled}\rvert$	η^{calc}	Atom
1	260	0.2	420	210	0.7	F7
2	260	0.2	380	190	0.5	F3
3	170	0.8	400	200	0.4	F2
			340	170	0.5	F6
4	170	0.8	350	180	0.5	F1
5	240	0.5	360	180	0.4	F4
6	240	0.5	390	190	0.1	F5

Two-dimensional DQ MAS NMR measurements were made to identify pairs of peaks in the ^{19}F NMR spectra corresponding to fluorine nuclei in close spatial proximity and therefore as a check on the peak assignments and an example of the results is shown in Figure 4. The DFT structure was used to identify the nearest neighbor fluorine atoms (4 Å cutoff) and their expected dipole-dipole couplings. The couplings are provided in Table 4. The strongest diagonal peaks are predicted for F3 and F5, and while the F5-F5 peak is clearly shown in Figure 4, the F3-F3 peak is not observed. However, the F3 peak also has weak intensity in the 1D projection of **Figure 4**. The absence of the peaks in the 1D projection is not unusual since typical DQ NMR sequences involve multiple imperfect pulses and long evolution times which can lead to signal losses, i.e., the effective T_2 varies from peak to peak, particularly for dense spin systems where peak intensities

are strongly affected by the multitude of interfering couplings.[17] In essence the 1D projection in a 2D DQ MAS experiment is not quantitative but instead provides a qualitative comparison. **Table 4** also predicts the following cross peaks, F7-F1, F7-F2, F1-F2, and F1-F6, all of which are observed. Therefore, the cross-peaks support the spectral assignments from DFT calculations. From the structure, the distances corresponding to the observed cross peaks are: 2.552 Å for F5-F5, 2.680 Å for F7-F1, 2.737 Å for F7-F2, 2.834 Å for F1-F2, 2.773 Å for F1-F6. These fluorine-fluorine interatomic distances are consistent with other metal oxyfluoride F-F distances characterized successful by 2D ^{19}F DQ-SQ MAS NMR methods.[36]

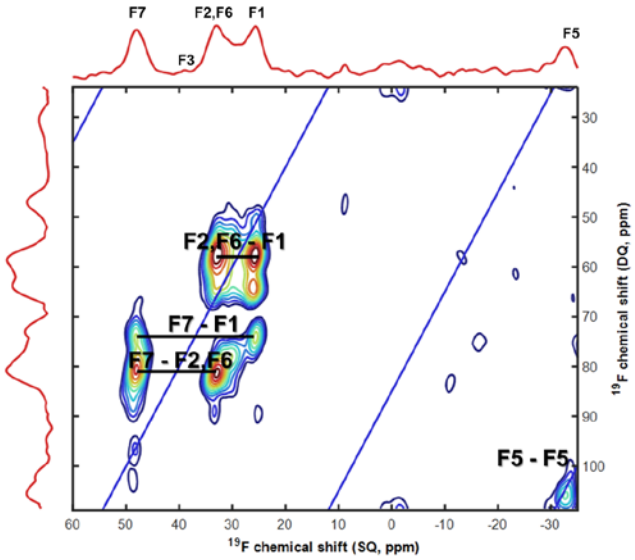

Figure 4: 2D ^{19}F DQ MAS spectrum obtained using a spinning frequency of 50 kHz. The solid blue line indicates the diagonal of the 2D spectrum for which the autocorrelation peaks appear. The projection of the 2D onto the ^{19}F SQ and DQ dimensions is shown on top and to the left, respectively.

Table 4: Calculated ^{19}F-^{19}F homonuclear dipolar couplings in kHz as extracted from structure obtained from DFT calculation. Only those pairs whose inter-nuclear distances are less than 4Å are listed.

	F1	F2	F3	F4	F5	F6	F7
F1		4.67	1.67			4.98	5.52
F2	4.67		5.11				5.19 2.28
F3	1.67	5.11	6.22				5.32
F4					4.82	4.40 5.24	
F5				4.82	6.39		
F6	4.98			4.40 5.24		1.80	
F7	5.52	5.19 2.28	5.32				

4. Conclusions

The ^{19}F chemical shifts of crystalline uranyl fluoride ($UO_2F_2 \cdot 1.57H_2O$) were investigated using solid-state NMR. While seven nonequivalent fluorine sites are found in the structure, the ^{19}F NMR spectra contained six peaks with peak shifts at -33.0, 9.1, 25.7, 33.0, 39.0, and 48.2 ppm. The calculated isotropic shielding tensors (σ_{iso}) for the fluorine sites allowed for assignment of ^{19}F NMR spectral features to specific fluorine sites. The peak at 33.0 ppm is consistent with two distinct sites. 2D ^{19}F DQ MAS NMR spectra were generally consistent with the peak assignments.

Supporting Information

The supporting information contains XRD, experimental, and calculation parameters for CASTEP.

Acknowledgements

The authors wish to thank Dr. Andrew Harter, staff scientist at Oak Ridge National Laboratory, for his contributing discussions. This work was funded by the Office of Defense Nuclear Nonproliferation Research and Development within the National Nuclear Security Administration for the U.S. Department of Energy. This work was supported by the Office of Naval Research. This manuscript has been authored by Savannah River Nuclear Solutions, LLC under Contract No. DE-AC09-08SR22470 with the U.S. Department of Energy. The United States Government retains and the publisher, by accepting this article for publication, acknowledges that the United States Government retains a non-exclusive, paid-up, irrevocable, worldwide license to publish or reproduce the published form of this work, or allow others to do so, for United States Government purposes.

;

References

1. Harris, R. K. W., R.E.; Duer, M.J, *NMR Crystallography*. Wiley: 2009; p 520.
2. Clark Stewart, J.; Segall Matthew, D.; Pickard Chris, J.; Hasnip Phil, J.; Probert Matt, I. J.; Refson, K.; Payne Mike, C., First Principles Methods Using CASTEP. *Z. Kristallogr.* **2005,** *220* (5/6), 567.
3. Schreckenbach, G., NMR Shielding Calculations Across the Periodic Table: Diamagnetic Uranium Compounds. 2. Ligand and Metal NMR. *Inorg. Chem.* **2002,** *41* (25), 6560-6572.
4. Schreckenbach, G.; Wolff, S. K.; Ziegler, T., NMR Shielding Calculations Across the Periodic Table: Diamagnetic Uranium Compounds. 1. Methods and Issues. *J. Phys. Chem. A* **2000,** *104* (35), 8244-8255.
5. Sadoc, A.; Biswal, M.; Body, M.; Legein, C.; Boucher, F.; Massiot, D.; Fayon, F., NMR Parameters in Column 13 Metal Fluoride Compounds (AlF_3, GaF_3, InF_3 and TlF) from First Principle Calculations. *Solid State Nucl. Magn. Reson.* **2014,** *59–60*, 1-7.
6. Sadoc, A.; Body, M.; Legein, C.; Biswal, M.; Fayon, F.; Rocquefelte, X.; Boucher, F., NMR Parameters in Alkali, Alkaline Earth and Rare Earth Fluorides from First Principle Calculations. *Phys. Chem. Chem. Phys.* **2011,** *13* (41), 18539-18550.
7. Cho, H.; de Jong, W. A.; Soderquist, C. Z., Probing the Oxygen Environment in UO_2^{2+} by Solid-state ^{17}O Nuclear Magnetic Resonance Spectroscopy and Relativistic Density Functional Calculations. *J. Chem. Phys.* **2010,** *132* (8), 084501.
8. Smith, A. L.; Raison, P. E.; Martel, L.; Charpentier, T.; Farnan, I.; Prieur, D.; Hennig, C.; Scheinost, A. C.; Konings, R. J. M.; Cheetham, A. K., A ^{23}Na Magic Angle Spinning Nuclear Magnetic Resonance, XANES, and High-Temperature X-ray Diffraction Study of $NaUO_3$, Na_4UO_5, and $Na_2U_2O_7$. *Inorg. Chem.* **2014,** *53* (1), 375-382.
9. Marchenko, A.; Truflandier, L. A.; Autschbach, J., Uranyl Carbonate Complexes in Aqueous Solution and Their Ligand NMR Chemical Shifts and ^{17}O Quadrupolar Relaxation Studied by ab Initio Molecular Dynamics. *Inorg. Chem.* **2017,** *56* (13), 7384-7396.
10. Alam, T. M.; Liao, Z.; Nyman, M.; Yates, J., Insight into Hydrogen Bonding of Uranyl Hydroxide Layers and Capsules by Use of ^1H Magic-Angle Spinning NMR Spectroscopy. *J. Phys. Chem. C* **2016,** *120* (19), 10675-10685.
11. Morato, F.; Fourcade, R.; Ducourant, B.; Feugier, A., Existence, Characterization and Decomposition of Uranyl Difluoride Hydrates. *Rev. Metall. / Cah. Inf. Tech.* **1999,** *96* (2), 163-168.
12. Armstrong, D. P.; Jarabek, R. J.; Fletcher, W. H., Micro-Raman Spectroscopy of Selected Solid $U_XO_YF_Z$ Compounds. *Appl. Spectrosc.* **1989,** *43* (3), 461-468.
13. Morato, F.; Fulconis, J. M.; Rouquérol, F.; Fourcade, R., Study of the Dehydration Process of Uranyl Difluoride Hydrates Stable Under Usual Conditions of Temperature, Pressure and Atmospheric Moisture. *J. Fluorine Chem.* **1998,** *91* (1), 69-73.
14. Lychev, A. A.; Mikhalev, V. A.; Suglobov, D. N., Crystalline Hydrates of Uranyl Fluoride at 20 °C. *Radiokhimiya* **1990,** *32*, 7-12.
15. Atoji, M.; McDermot.Mj, Crystal Structure of Anhydrous UO_2F_2. *Acta Crystallogr. Sect. B: Struct. Sci.* **1970,** *B 26* (OCT15), 1540.
16. Mikhailov, Y. N.; Gorbunova, Y. E.; Stolyarov, I. P.; Moiseev, I. I., Synthesis and Structure of a New Modification of Monoaquadifluorouranyl Hydrate. *Russ. J. Inorg. Chem.* **2002,** *47*, 1821-1826.

17. Schnell, I., Dipolar Recoupling in Fast-MAS Solid-state NMR Spectroscopy. *Prog. Nucl. Magn. Reson. Spectrosc.* **2004,** *45* (1–2), 145-207.
18. Feike, M., Demco, D.E., Graf, R., Gottwald, J., Hafner, S., Broadband Multiple-Quantum NMR Spectroscopy. *J. Magn. Reson. A* **1996,** *122*, 214-221.
19. Perdew, J. P.; Burke, K.; Ernzerhof, M., Generalized Gradient Approximation Made Simple. *Phys. Rev. Lett.* **1996,** *77* (18), 3865-3868.
20. Vanderbilt, D., Soft Self-Consistent Pseudopotentials in a Generalized Eigenvalue Formalism. *Phys. Rev. B: Condens. Matter* **1990,** *41* (11), 7892-7895.
21. Straka, M.; Kaupp, M., Calculation of ^{19}F NMR Chemical Shifts in Uranium Complexes Using Density Functional Theory and Pseudopotentials. *Chem. Phys.* **2005,** *311* (1), 45-56.
22. Zheng, A.; Liu, S.-B.; Deng, F., 19F Chemical Shift of Crystalline Metal Fluorides: Theoretical Predictions Based on Periodic Structure Models. *J. Phys. Chem. C* **2009,** *113* (33), 15018-15023.
23. Griffin, J. M.; Yates, J. R.; Berry, A. J.; Wimperis, S.; Ashbrook, S. E., High-Resolution 19F MAS NMR Spectroscopy: Structural Disorder and Unusual J Couplings in a Fluorinated Hydroxy-Silicate. *J. Am. Chem. Soc.* **2010,** *132* (44), 15651-15660.
24. Martineau, C.; Allix, M.; Suchomel, M. R.; Porcher, F.; Vivet, F.; Legein, C.; Body, M.; Massiot, D.; Taulelle, F.; Fayon, F., Structure Determination of Ba_5AlF_{13} by Coupling Electron, Synchrotron and Neutron Powder Diffraction, Solid-state NMR and ab Initio Calculations. *Dalton Trans.* **2016,** *45* (39), 15565-15574.
25. Martineau, C.; Fayon, F.; Suchomel, M. R.; Allix, M.; Massiot, D.; Taulelle, F., Structure Resolution of $Ba_5Al_3F_{19}$ and Investigation of Fluorine Ion Dynamics by Synchrotron Powder Diffraction, Variable-Temperature Solid-State NMR, and Quantum Computations. *Inorg. Chem.* **2011,** *50* (6), 2644-2653.
26. Rollet, A.-L.; Allix, M.; Veron, E.; Deschamps, M.; Montouillout, V.; Suchomel, M. R.; Suard, E.; Barre, M.; Ocaña, M.; Sadoc, A.; Boucher, F.; Bessada, C.; Massiot, D.; Fayon, F., Synthesis and Structure Resolution of $RbLaF_4$. *Inorg. Chem.* **2012,** *51* (4), 2272-2282.
27. Yi, H.; Balan, E.; Gervais, C.; Segalen, L.; Fayon, F.; Roche, D.; Person, A.; Morin, G.; Guillaumet, M.; Blanchard, M.; Lazzeri, M.; Babonneau, F., A Carbonate-fluoride Defect Model for Carbonate-rich Fluorapatite. *Am. Mineral.* **2013,** *98* (5-6), 1066.
28. Pedone, A.; Charpentier, T.; Menziani, M. C., The Structure of Fluoride-containing Bioactive Glasses: New Insights from First-principles Calculations and Solid State NMR Spectroscopy. *J. Mater. Chem.* **2012,** *22* (25), 12599-12608.
29. Dabachi, J.; Body, M.; Dittmer, J.; Fayon, F.; Legein, C., Structural Refinement of the RT LaOF Phases by Coupling Powder X-Ray Diffraction, ^{19}F and ^{139}La Solid State NMR and DFT Calculations of the NMR Parameters. *Dalton Trans.* **2015,** *44* (47), 20675-20684.
30. Neouze, M.-A.; Kronstein, M.; Litschauer, M.; Puchberger, M.; Coelho, C.; Bonhomme, C.; Gervais, C.; Tielens, F., Exploring the Molecular Structure of Imidazolium–Silica-Based Nanoparticle Networks by Combining Solid-State NMR Spectroscopy and First-Principles Calculations. *Chem. Eur. J.* **2014,** *20* (46), 15188-15196.
31. Sene, S.; Berthomieu, D.; Donnadieu, B.; Richeter, S.; Vezzani, J.; Granier, D.; Begu, S.; Mutin, H.; Gervais, C.; Laurencin, D., A Combined Experimental-computational Study of Benzoxaborole Crystal Structures. *CrystEngComm* **2014,** *16* (23), 4999-5011.
32. Arnold, A. A.; Terskikh, V.; Li, Q. Y.; Naccache, R.; Marcotte, I.; Capobianco, J. A., Structure of $NaYF_4$ Upconverting Nanoparticles: A Multinuclear Solid-State NMR and DFT Computational Study. *J. Phys. Chem. C* **2013,** *117* (48), 25733-25741.

33. Miskowiec, A., Kirkegaard, M.C., Herwig, K.W., Trowbridge, L., Mamontov, E., Anderson, B., Quasielastic Neutron Scattering with in situ Humidity Control: Water Dynamics in Uranyl Fluoride. *J. Appl. Phys.* **2016,** *119*, 094308.
34. Bak, M.; Rasmussen, J. T.; Nielsen, N. C., SIMPSON: A General Simulation Program for Solid-State NMR Spectroscopy. *J. Magn. Reson.* **2000,** *147* (2), 296-330.
35. Laskowski, R.; Blaha, P.; Tran, F., Assessment of DFT Functionals with NMR Chemical Shifts. *Phys. Rev. B: Condens. Matter* **2013,** *87* (19), 195130.
36. Alam, T. M. C., J.S.; Bonhomme, F.; Thoma, S.G.; Rodriquez, M.A.; Zheng, S.; Autschbach, J., A Solid-State NMR, X-ray Diffraction, and Ab Initio Investigation into the Structures of Novel Tantalum Oxyfluoride Clusters. *Chem. Mater.* **2008,** *20*, 2205-2217.

TOC Graphic